

Charged particle tracking via edge-classifying interaction networks

Gage DeZoort^{1,*}, Savannah Thais^{1,**}, Isobel Ojalvo¹, Peter Elmer¹, Vesal Razavimaleki², Javier Duarte², Markus Atkinson³, and Mark Neubauer³

¹Princeton University, Princeton, NJ, USA

²University of California San Diego, La Jolla, CA, USA

³University of Illinois at Urbana-Champaign, Champaign, IL, USA

Abstract. Recent work has demonstrated that geometric deep learning methods such as graph neural networks (GNNs) are well-suited to address a variety of reconstruction problems in HEP. In particular, tracker events are naturally represented as graphs by identifying hits as nodes and track segments as edges; given a set of hypothesized edges, edge-classifying GNNs predict which correspond to real track segments. In this work, we adapt the physics-motivated interaction network (IN) GNN to the problem of charged-particle tracking in the high-pileup conditions expected at the HL-LHC. We demonstrate the IN's excellent edge-classification accuracy and tracking efficiency through a suite of measurements at each stage of GNN-based tracking: graph construction, edge classification, and track building. The proposed IN architecture is substantially smaller than previously studied GNN tracking architectures, a reduction in size critical for enabling GNN-based tracking in constrained computing environments. Furthermore, the IN is easily expressed as a set of matrix operations, making it a promising candidate for acceleration via heterogeneous computing resources.

1 Introduction

Charged particle tracking is essential to many downstream reconstruction tasks including vertex finding [1, 2], particle reconstruction [3, 4], and jet flavor tagging [5–7]. Current tracking algorithms at the CERN Large Hadron Collider (LHC) experiments [8, 9] are typically based on the combinatorial Kalman filter [10–13] and have been shown to scale worse than linearly with increasing beam intensity and detector occupancy [14]. The high-luminosity phase of the LHC (HL-LHC) will see an order of magnitude increase in luminosity [15], highlighting the need to develop new tracking algorithms demonstrating reduced latency and improved performance in high-pileup environments. To this end, ongoing research focuses on both accelerating current tracking algorithms via dedicated hardware or parallelization and developing new tracking algorithms with machine learning (ML) techniques.

Geometric deep learning (GDL) [16–19] is a growing sub-field of ML focused on learning representations on non-Euclidean domains such as sets, graphs, and manifolds. Graph neural

*e-mail: jdezoort@princeton.edu

**e-mail: sthais@princeton.edu

networks (GNNs) [20–25] are the subset of GDL algorithms that run on graphs, data represented as a set of nodes connected by edges. Tracker data is naturally represented as a graph; hits form a 3D point cloud and the edges between them represent hypotheses about particle trajectories. Recent progress by the Exa.TrkX project and other collaborations has demonstrated that edge-classifying GNNs are well-suited to particle tracking applications [26–28]. Tracking via edge classification typically involves three stages. In the graph construction stage, tracker hits are mapped to nodes and an edge-assignment algorithm forms edges between certain nodes. In the edge classification stage, an edge-classifying GNN infers the probability that each edge corresponds to a true track segment. Finally, in the track building step, a track-building algorithm leverages the edge weights to form full track candidates.

In this work, we present a suite of measurements at each of these stages, exploring a range of strategies and algorithms to facilitate GNN tracking. We focus in particular on the interaction network (IN) [23], a GNN architecture frequently used as a building block in more complicated architectures [26, 28]. The IN itself demonstrates powerful edge-classification capability, and its simple matrix formulation makes it a promising candidate for acceleration via heterogeneous computing resources [29]. In Section 2, we first present an overview of particle tracking and graph-based representations of track hits. In Section 3, we introduce INs and describe the mathematical foundations of our architecture. In Section 4, we present specific graph construction, IN edge classification, and track building measurements on the TrackML dataset. Additionally, we present IN inference time measurements, framing this work in the context of ongoing GNN acceleration studies. In Section 5, we summarize the results of our studies and contextualize them in the broader space of ML-based particle tracking. We conclude in the same section with outlook and discussion of future studies, in particular highlighting efforts to accelerate INs via heterogeneous computing resources.

2 Theory and Background

2.1 Particle Tracking

In collider experiments such as the LHC, charged particle trackers are comprised of cylindrical detector layers immersed in an axially-aligned magnetic field. The detector geometry is naturally specified by cylindrical coordinates (r, ϕ, z) , where the z axis is aligned with the beamline. Pseudorapidity is a measure of angle with respect to the beamline, defined as $\eta = -\log \tan \frac{\theta}{2}$ where θ is the polar angle. Charged particles produced in collision events move in helical trajectories through the magnetic field, generating localized hits in the tracker layers via ionization energy deposits. Track reconstruction consists of “connecting the dots,” wherein hits are systematically grouped to represent charged particle trajectories. We refer to a pair of hits that belong to the same particle as a track segment, such that the line extending between the hits is a linear approximation of the particle’s trajectory. Reconstructed tracks are defined by their respective hit patterns and kinematic properties, which are extracted from each track’s helix parameters. Specifically, initial position and direction follow directly from helical fits and the transverse momentum p_T is extracted from the track’s curvature [30].

In this work, we focus specifically on track finding in the pixel detector, the innermost subdetector of the tracker. Many tracking algorithms run “inside out,” where track seeds from the pixel detector are used to estimate initial track parameters and propagated through the full detector [8]. Improving the seeding stage of the tracking pipeline is an important step towards enabling efficient tracking at the HL-LHC; this approach is complimentary to other GNN-based tracking efforts that focus on the full tracker barrel (without including endcaps) using graph segmentation [27].

2.2 Tracker Hits as Graphs

Tracking data is naturally represented as a graph by identifying hits as nodes and track segments as (in general) directed edges. In this scheme, nodes have cylindrical spatial features $x_i = (r_i, \phi_i, z_i)$ and edges are represented by two adjacency matrices: $R_i, R_o \in \mathbb{R}^{n_{\text{edges}} \times n_{\text{nodes}}}$. The elements $(R_i)_{e,h}$ are 1 if edge e is incoming to hit h and 0 otherwise. R_o is defined similarly for outgoing edges. Each edge is assigned a set of geometric features $e_{ij} = (\Delta r_{ij}, \Delta \phi_{ij}, \Delta z_{ij}, \Delta R_{ij})$, where $\Delta R_{ij} = \sqrt{\Delta \eta_{ij}^2 + \Delta \phi_{ij}^2}$. These relations are stacked into matrices $X = [x_i] \in \mathbb{R}^{n_{\text{nodes}} \times 3}$ and $R_a = [e_{ij}] \in \mathbb{R}^{n_{\text{edges}} \times 4}$. Accordingly, we define a *hitgraph* representing tracking data as $\mathcal{G} := (X, R_a, R_i, R_o)$. The corresponding training target is the vector $y \in \mathbb{R}^{n_{\text{edges}}}$, whose components y_e are 1 when edge e is a true track segment and 0 otherwise.

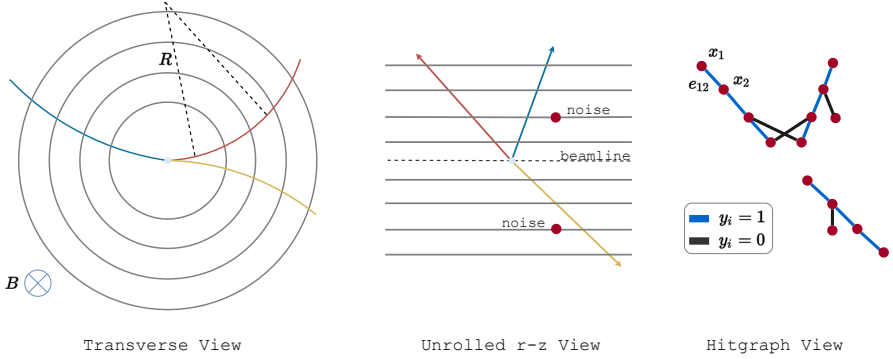


Figure 1: (Left) A transverse view of a generic particle tracker. The magnetic field is aligned with the z -axis such that tracks move with a radius of curvature R in the transverse plane, yielding measurements of transverse momentum via $p_T = 0.3 \left[\frac{\text{GeV}}{\text{T}\cdot\text{m}} \right] BR$. (Middle) The tracker barrel layers are unrolled in the r - z plane to show the full three-particle plus noise event. (Right) The corresponding hitgraph is shown with example node and edge labels.

3 Interaction Networks

The IN is a physics-motivated GNN capable of reasoning about objects and their relations [23]. Each IN forward-pass involves a relational reasoning step, in which an interaction is computed, and an object reasoning step, in which interaction effects are aggregated and object dynamics are applied. The resulting predictions have been shown to generate next-timestep dynamics consistent with various physical principles. We adapt the IN to the problem of edge classification by conceptualizing each hitgraph as a complex network of hit “objects” and hypothesized edge “relations.” In this context, the relational and object reasoning steps correspond to edge and node re-embeddings respectively. In an edge classification scheme, the IN must determine whether or not each hitgraph edge represents a track segment. Accordingly, we extend the IN forward pass to include an additional relational reasoning step, which produces an edge weight for each hypothesized edge in the hitgraph.

3.1 Mathematical Formulation

The IN forward pass begins with an input hitgraph $\mathcal{G} = (X, R_a, R_i, R_o)$. The hits receiving an incoming edge are given by $X_i := R_i X \in \mathbb{R}^{n_{\text{edges}} \times 3}$; likewise, the hits sending an outgoing

edge are given by $X_o := R_o X \in \mathbb{R}^{n_{\text{edges}} \times 3}$. Interaction terms are defined by the concatenation $m(\mathcal{G}) := [X_i, X_o, R_a] \in \mathbb{R}^{n_{\text{edges}} \times 10}$, known as the marshalling step. A relational network $\phi_R^{(1)}$ predicts an ‘‘effect’’ for each interaction term, $E := \phi_R^{(1)}(m(\mathcal{G})) \in \mathbb{R}^{n_{\text{edges}} \times 4}$. These effects are aggregated via summation for each receiving node, $A := a(\mathcal{G}, E) = R_i^T E \in \mathbb{R}^{n_{\text{nodes}} \times 4}$, and concatenated with X to form a set of expanded hit features $C := [X, A] \in \mathbb{R}^{n_{\text{nodes}} \times 7}$. An object network ϕ_O re-embeds the hit positions as $\tilde{X} := \phi_O(C) \in \mathbb{R}^{n_{\text{nodes}} \times 3}$. At this point, the traditional IN inference is complete, having re-embedded both the edges and nodes. Accordingly, we denote the re-embedded graph $\text{IN}(\mathcal{G}) = \tilde{\mathcal{G}} = (\tilde{X}, E, R_i, R_o)$.

In order to produce edge weights to be used in the track-building algorithm an additional relational reasoning step is performed on $\tilde{\mathcal{G}}$. The marshalling step yields new interaction terms $m(\tilde{\mathcal{G}}) = [\tilde{X}_i, \tilde{X}_o, E] \in \mathbb{R}^{n_{\text{edges}} \times 10}$ and a second relational network $\phi_R^{(2)}$ predicts edge weights for each edge: $W := \phi_R^{(2)}(m(\tilde{\mathcal{G}})) \in (0, 1)^{n_{\text{edges}}}$. Summarily, we have a full forward pass of the edge classification IN:

$$W(\mathcal{G}) = \phi_R^{(2)} \left[m(\text{IN}(\mathcal{G})) \right] = \phi_R^{(2)} \left[m \left(\mathcal{G}, \phi_O \left[\mathcal{G}, a(\mathcal{G}, \phi_R^{(1)} [m(\mathcal{G})) \right] \right) \right] \quad (1)$$

4 Measurements

4.1 TrackML Dataset

The TrackML dataset is a simulated set of proton-proton collision events originally developed for the TrackML Particle Tracking Challenge [31]. TrackML events are generated with 200 pileup interactions on average, simulating the high-pileup conditions expected at the HL-LHC. Each event contains 3D hit position and truth information about the particles that generated them. In particular, particles are specified by particle IDs (p_{ID}) and three-momentum vectors (\mathbf{p}).

The TrackML detector is designed as a generalized LHC tracker; it contains discrete layers of sensor arrays immersed in a strong magnetic field. We focus specifically on the pixel layers, a highly-granular set of four barrel and fourteen endcap layers in the innermost tracker regions. The pixel layers are shown in Figure 2. We note that constraining our studies to the pixel layers reduces the size of the hitgraphs such that the full graph can be held in memory and processed by the GNN without segmentation.

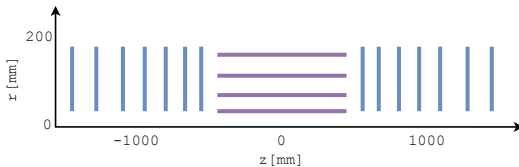


Figure 2. The pixel detector is a set of highly-granular layers sitting in the innermost region of the TrackML detector.

4.2 Graph Construction

In the graph construction stage, each event’s tracker hits are converted to a hitgraph of the form $\mathcal{G} = (X, R_a, R_i, R_o)$. Typically, a set of filters are applied to hits before they are assigned to graph nodes. For example, p_T filters reject hits generated by particles with $p_T < p_T^{\text{min}}$, noise filters reject noise hits, and same-layer filters reject all but one hit per layer for each particle. After initial hit filtering yields a set of nodes, edge-assignment algorithms extend edges between certain nodes. These edges are inputs to the inference stage and must therefore represent as many true track segments as possible. Towards this goal, one might naively

Table 1: Configuration parameters for the graph construction methods at each p_T^{\min} . Note that while the HEP.TrkX+ and DBSCAN share the same ϕ_{slope} and z_0 parameters, DBSCAN requires two additional clustering parameters: ϵ , which defines the neighborhood radius, and MinPts , the number of points required to seed a cluster.

p_T^{\min} [GeV]	HEP.TrkX		HEP.TrkX+, DBSCAN		DBSCAN	
	ϕ_{slope} [10^{-4}]	z_0 [m]	ϕ_{slope} [10^{-4}]	z_0 [m]	ϵ	MinPts
2	6	0.1	6	15	0.22	3
1.5	6	0.1	6	15	0.18	3
1	6	0.1	6	15	0.1	3
0.75	7.63	0.1	7.63	25	0.08	3
0.6	7.63	0.1	7.63	29.5	0.06	3
0.5	7.63	0.1	7.63	29.5	0.05	3

return a fully-connected hitgraph. However, this strategy yields $\frac{1}{2}n_{\text{nodes}}(n_{\text{nodes}} - 1)$ edges, which for $n_{\text{nodes}} \sim \mathcal{O}(1,000)$ gives $n_{\text{edges}} \sim \mathcal{O}(500,000)$. This represents a fundamental trade-off between different edge-assignment algorithms: they must simultaneously maximize *truth efficiency*, the fraction of track segments represented as true edges, and *edge efficiency*, the fraction of true edges to total edges in the hitgraph.

In this work, we compare multiple graph construction algorithms, each of which determines whether or not to extend an edge e_{ij} between hits x_i and x_j . In all methods, only pixel detector hits are considered, pseudorapidity is restricted to $\eta \in [-5, 5]$, and the noise and same-layer hit filters are applied. The same-layer filter introduces an ambiguity in defining edges between the barrel and innermost endcap layers. Specifically, barrel hits generated by the same particle could produce multiple true edges incoming to a single endcap hit. The resulting triangular edge pattern conflicts with the main assumption of the same-layer filter, that only one true track segment exists between each subsequent layer. For this reason, a *barrel intersection* cut was developed, in which edges between a barrel layer and an innermost endcap layer are rejected if they intersect with any intermediate barrel layers.

In the following studies, the p_T filter is varied to modulate the graph size (see Fig. 3) and cuts on the geometric quantities $z_0 = z_i - r_i \frac{z_j - z_i}{r_j - r_i}$ and $\phi_{\text{slope}} = \frac{\phi_j - \phi_i}{r_j - r_i}$ are used to reject edges. We compare three graph construction methods:

1. HEP.TrkX (barrel only): Edges must satisfy z_0 and ϕ_{slope} constraints.
2. HEP.TrkX+ (barrel+endcaps): Edges must satisfy z_0 and ϕ_{slope} constraints and the barrel intersection cut.
3. DBSCAN (barrel+endcaps): In addition to all HEP.TrkX+ cuts, edges must also belong to the same cluster in η - ϕ space determined by the density-based spatial clustering of applications with noise (DBSCAN) algorithm [32].

A summary of the parameters used for each graph construction method is given in Tab. 1; key metrics corresponding to these graph construction algorithms are shown in Fig. 4. The results indicate that incorporating the endcaps leads to drops in both truth and edge efficiency with corresponding increases in n_{edges} and n_{nodes} . This suggests that simple geometric cuts are increasingly unable to filter false edges as broader detector information is introduced, further highlighting the need for GNN edge-classification. Note that the DBSCAN truth efficiency is upper bounded by the HEP.TrkX+ method's, but in general the DBSCAN edge efficiency is substantially higher. This reflects the fact that same-track hits are likely to be clustered

in η - ϕ space, such that even clusters capturing many different particles form a solid basis from which to construct edges. For the remainder of the studies in this paper we focus on the HEP.TrkX+ graph construction method.

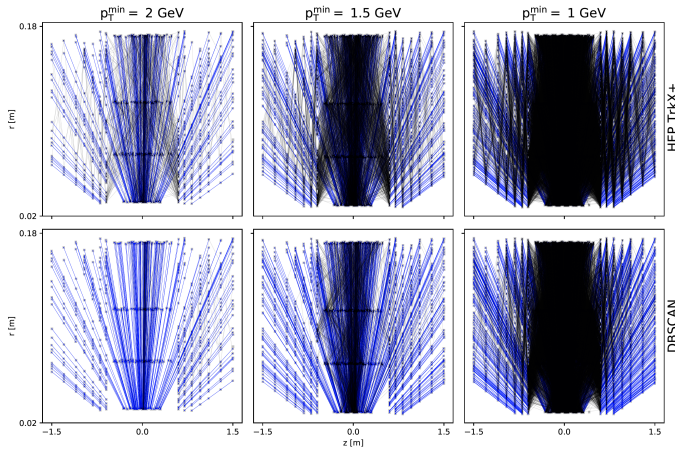


Figure 3. As p_T^{\min} is decreased, graphs are increasingly composed of false edges; pre-clustering hits in η - ϕ space reduces the fraction of false edges, thereby increasing edge efficiency.

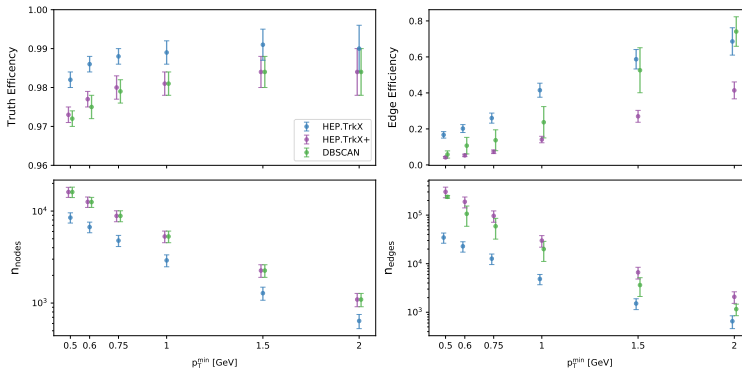


Figure 4: Measurements of truth efficiency (top left), edge efficiency (top right), number of nodes per graph (bottom left) and number of edges per graph (bottom right) as a function of p_T^{\min} . Some data points are slightly offset along the x -axis for visual effect only.

4.3 Edge Classification

Towards transparency and applicability to future acceleration studies, we have implemented the IN in PyTorch [33] as the set of explicit matrix multiplications, concatenations, and transposes detailed in Sec. 3. The full forward-pass, comprised of edge and node re-embeddings used to predict edge weights, is shown in Fig. 5 below. The functions $\phi_R^{(1)}$, $\phi_R^{(2)}$, and ϕ_O are approximated as multilayer perceptrons (MLPs) with rectified linear unit (ReLU) activation functions [34, 35]. The ReLU activation function behaves as an identity function for positive inputs and saturates at 0 for negative inputs. Notably, the $\phi_R^{(2)}$ outputs have a sigmoid activation $\sigma(\cdot) \in (0, 1)$, such that they represent probabilities, or edge weights, $W(\mathcal{G}) \in (0, 1)^{n_{\text{edges}}}$ that each edge is a track segment. We therefore seek to optimize a binary cross-entropy (BCE)

loss between the truth targets $y_i = \{0, 1\}$ and edge weights $w_i \in (0, 1)$:

$$\ell(y_n, W_n(\mathcal{G})) = - \sum_{i=1}^{n_{\text{edges}}} (y_i \log w_i + (1 - y_i) \log(1 - w_i)) \quad (2)$$

Here, n is the sample index, so that the total loss per epoch is the average BCE loss $L(\{\mathcal{G}_n, y_n\}_{n=1}^N) = \frac{1}{N} \sum_{n=1}^N \ell(y_n, W_n(\mathcal{G}))$. Throughout the following studies, the architecture in Fig. 5 is held at a constant size of 6,448 trainable parameters, corresponding to 40 hidden units per layer in each of the MLPs. Validation studies indicated that even this small network rapidly converged to losses at or below $\mathcal{O}(10^{-2})$, similar to its larger counterparts (see Fig. 5). Specifically, we train graphs produced via the HEP.TrkX+ method with p_T^{min} ranging from 0.6–2 GeV. At each value of p_T^{min} , 1500 graphs belonging to the TrackML `train_1` sample were randomly divided into 1000 training, 400 testing, and 100 validation samples. To facilitate training, we use the Adam optimizer [36] with a learning rate of 0.005, which is decayed by a factor of $\gamma = 0.9$ every 5 epochs.

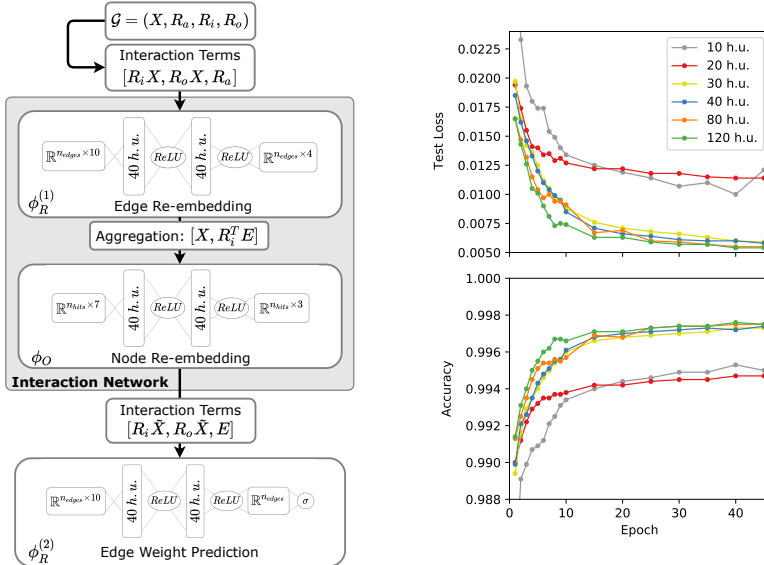


Figure 5: (Left) The complete IN forward-pass with the relational and object models approximated as MLPs. (Right) An example hyperparameter scan, in which a models with varying numbers of hidden units (h.u.) were trained on $p_T^{\text{min}} = 1$ GeV graphs.

In order to evaluate the IN edge-classification performance, it is necessary to define a threshold δ such that each edge weight $w_i \in W(\mathcal{G})$ satisfying $w_i \geq \delta$ or $w_i < \delta$ indicates that edge i was classified as true or false respectively. Here, we define δ^* as the threshold at which the true positive rate (TPR) equals the true negative rate (TNR). In principle, δ^* may be calculated individually for each graph. However, this introduces additional overhead to the inference step, which is undesirable in constrained computing environments. We instead determine δ^* during the training process by minimizing the difference $|\text{TPR} - \text{TNR}|$ for graphs in the validation set. The resulting δ^* , which is stored for use in evaluating the testing sample, represents the average optimal threshold for the validation graphs. Accordingly, we define the model’s accuracy at δ^* as $(n_{\text{TP}} + n_{\text{TN}})/n_{\text{edges}}$, where n_{TP} (n_{TN}) is the number of true positives (negatives), and note that the BCE loss is independent of δ^* .

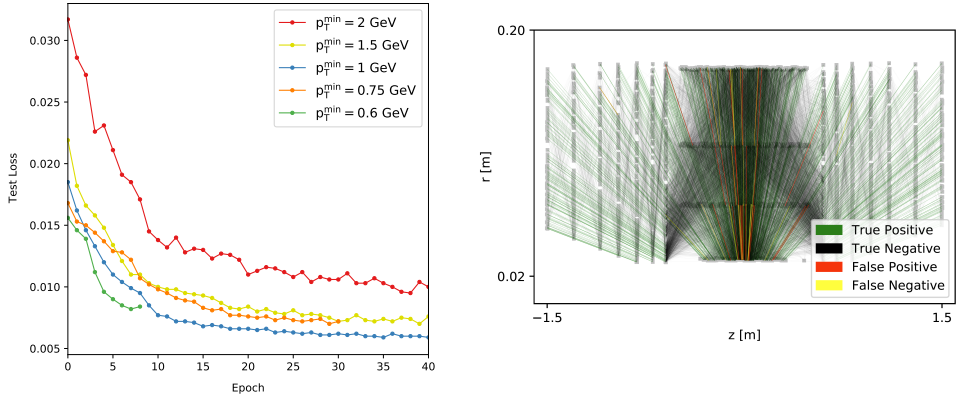


Figure 6: (Left) Loss convergence for models trained on various p_T^{\min} graphs. (Right) A model trained on $p_T^{\min} = 1$ GeV graphs was used to evaluate an unseen $p_T^{\min} = 1$ GeV graph, yielding a loss of 6.0×10^{-3} and accuracy of 99.81%. 57 out of 29,661 edges were incorrectly classified; these erroneous classifications are magnified in the figure.

Edge-Classification Accuracy

Training p_T^{\min} [GeV]	2	1.5	1	0.75	0.6
2	0.9965(29)	0.9963(17)	0.9906(12)	0.9802(32)	0.9768(46)
1.5	0.9962(32)	0.9975(13)	0.9934(10)	0.9868(10)	0.9799(18)
1	0.9945(40)	0.9968(16)	0.9973(06)	0.9931(07)	0.9842(08)
0.75	0.9918(61)	0.9952(23)	0.9965(09)	0.9960(05)	0.9932(05)
0.6	0.9881(79)	0.9926(30)	0.9947(10)	0.9953(05)	0.9943(05)
	2	1.5	1	0.75	0.6
	Testing p_T^{\min} [GeV]				

Figure 7. Models trained on various p_T^{\min} graphs in the `train_1` sample were tested on 500 graphs from the `train_2` sample at various p_T^{\min} thresholds.

As shown in Figs. 6 and 7, the training process results in smooth convergence to excellent edge-classification accuracy. In particular, Fig. 7 shows that models trained on different p_T^{\min} demonstrate relatively robust performance on test sets with various p_T^{\min} , a critical performance criteria for tracking applications.

4.4 Track Building

In the track building step, the predicted edge weights $w_i \in W(\mathcal{G})$ are used to infer that edges satisfying $w_i \geq \delta^*$ represent true track segments. If the edge weight mask perfectly reproduced the training target (i.e. $\text{int}(W(\mathcal{G}) \geq \delta^*) = y$), the edge-classification step would produce $n_{\text{particles}}$ disjoint subgraphs, each corresponding to a single particle. Imperfect edge-classification leads to spurious connections between these subgraphs, prompting the need for more sophisticated track-building algorithms. Here, we use the union-find algorithm [37] and DBSCAN to cluster hits in the edge-weighted graphs.

We define three tracking efficiency measurements using progressively tighter requirements to allow comparison with current tracking algorithm efficiencies and other on-going HL-LHC tracking studies.

1. Cluster efficiency: the number of found clusters where all hits within the cluster originate from the same particle, divided by the total number of found clusters.
2. Physics efficiency: the number of found clusters where at least 50% of hits originate from the same particle and at least 50% of the corresponding particle’s hits are represented in the cluster, divided by the number of particles in the event.
3. Tight efficiency: the number of found clusters where all hits within the cluster originate from the same particle and the number of hits in the cluster matches the total number of hits generated by the particle, divided by the number of particles in the event.

Fig. 8 shows each of these tracking efficiencies as a function of p_T^{\min} for both the DBSCAN and union-find clustering approaches. In line with the performance of current tracking algorithms [8], the tracking efficiency increases with increasing p_T^{\min} , and levels off around 1.5 GeV to a maximum of approximately 99% cluster efficiency, 97% physics efficiency, and 95% tight efficiency. DBSCAN demonstrates higher tracking efficiency than union-find across all p_T values and efficiency definitions; the performance gap is larger for lower p_T values.

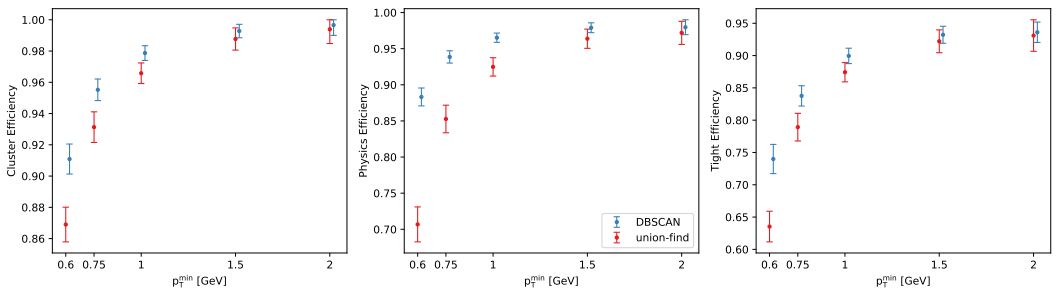


Figure 8: Track finding efficiencies with DBSCAN and union-find clustering for three efficiency definitions. Note that some data points are offset along the x-axis for visual effect only.

4.5 Inference Timing

An important advantage of GNN-based approaches over traditional methods for HEP reconstruction is the ability to natively run on highly parallel computing architectures. The PyTorch library [33] natively supports graphics processing units (GPUs) to parallelize the algorithm execution. For the IN studied in this work, the average CPU and GPU inference times per graph for a variety of minimum p_T cuts is shown in Table 2. As can be seen, inference can be significantly sped up with heterogeneous resources like GPUs. For instance, for a 1 GeV minimum p_T cut, the inference time for the HEP.TrkX+ graphs can be reduced by nearly a factor of 20 using the GPU with respect to the CPU. Other heterogeneous computing resources specialized for inference may be even more beneficial. This speed up may benefit the experiments’ computing workflows by accessing these resources as an on-demand, scalable service [38–40].

Table 2: CPU and GPU inference time estimates for each p_T threshold. The timing test were performed with an Nvidia Titan Xp GPU with 12 GB RAM and a 12-core Intel Xeon CPU E5-2650 v4 @ 2.20 GHz. Inference is performed with a batch size of one graph. The inference is repeated 100 times (after some warm-up) and the best time per inference is found. The mean and standard deviation of the best inference time derived for 5 random graphs in the testing dataset is then reported. For p_T^{\min} of 0.5 and 0.6 GeV, the inference could not be performed with the 12 GB RAM available on the GPU, as indicated with “—” in the table.

p_T^{\min} [GeV]	HEP.TrkX		HEP.TrkX+	
	CPU [ms]	GPU [ms]	CPU [ms]	GPU [ms]
2	1.5 ± 0.2	0.8 ± 0.02	2.9 ± 0.6	0.9 ± 0.03
1.5	2.8 ± 0.1	0.8 ± 0.01	13.1 ± 5.5	1.0 ± 0.2
1	11.1 ± 3.5	1.0 ± 0.1	130.7 ± 60.7	8.0 ± 4.0
0.75	44.6 ± 18.0	2.9 ± 1.3	686.2 ± 281.2	44.3 ± 18.8
0.6	131.0 ± 42.9	8.4 ± 2.7	1954.0 ± 724.7	—
0.5	250.2 ± 77.8	16.0 ± 5.2	1952.0 ± 717.0	—

Work has also been done to accelerate the inference of deep neural networks with heterogeneous resources beyond GPUs, like field-programmable gate arrays (FPGAs) [41–49]. This work extends to GNN architectures [28, 50]. Specifically, in Ref. [28], a compact version of the IN was implemented for $p_T > 2$ GeV segmented HEP.TrkX+ graphs with up to 28 nodes and 37 edges, and shown to have a latency less than $1 \mu\text{s}$, reproduce the floating-point precision model with a fixed-point precision of 16 bits or less, and fit on a Xilinx Kintex UltraScale FPGA.

While this preliminary FPGA acceleration work is promising, there are several limitations of the current FPGA implementation of the IN:

1. The design does not easily scale to beyond $\mathcal{O}(100)$ nodes and $\mathcal{O}(1,000)$ edges.
2. The neural network itself is small, and while it is effective for $p_T > 2$ GeV graphs, it may not be sufficient for lower- p_T graphs.
3. The FPGA design makes no assumptions about the possible graph connectivity (e.g. layer 1 nodes are only connected to layer 2 nodes), and instead allows all nodes to potentially participate in message passing. However by taking this additional structure into account, the hardware resources can be significantly reduced.
4. Quantization-aware training [47, 51–60] using QKERAS [48, 61] or BREVITAS [42, 62], parameter pruning [63–68], and general hardware-algorithm codesign can significantly reduce the necessary FPGA resources by reducing the required bit precision and removing irrelevant operations.
5. The design can be made more flexible, configurable, and reusable by integrating it fully with a user-friendly interface like h1s4m1 [69].

5 Summary and Outlook

In this work, we have shown that the physics-motivated IN is well-suited to the task of charged particle tracking in the high-pileup conditions expected at the HL-LHC. Through a suite of graph construction, edge classification, and track building measurements, we have framed

the IN's performance in the context of a complete GNN-based tracking pipeline. The graph construction measurements demonstrated that both the HEP.TrkX+ and DBSCAN graph construction methods achieve high truth efficiency in constructing graphs from pixel barrel and endcap layers; although the overall edge efficiency decreases with p_T for both methods, the graphs were found to be suitable for IN inference. The lightweight IN models trained in the edge classification step demonstrated extremely high edge classification efficiency for a range of p_T values. The track building measurements compared DBSCAN and union-find clustering on edge-weighted graphs to measure track building efficiency, demonstrating that DBSCAN outperforms union-find across the full p_T range for every efficiency metric.

The IN architecture presented here is substantially smaller than previous GNN tracking architectures, which may enable its use in constrained computing environments. Accordingly, we have compared the IN's CPU and GPU inference times and discussed related work on accelerating INs with FPGAs. As described in Section 4.5, there are several limitations to the current FPGA implementation of the IN and addressing these concerns is the subject of ongoing work.

Another important aspect of GNN-based tracking is reducing the time it takes to construct graphs. Ongoing efforts are dedicated to studying how best to accelerate graph construction using heterogeneous resources. Alternative GNN approaches that do not require an input graph structure, such as dynamic graph convolutional neural networks [25], distance-weighted GNNs [70], attention-based transformers [71], reformers [72], and performers [73], may be fruitful avenues of investigation as well.

In summary, geometric deep learning methods are well-suited to many physics reconstruction tasks, and our work and related studies establish GNNs as an extremely promising candidate for tracking at the HL-LHC.

Acknowledgement

S. T. and V. R. are supported by IRIS-HEP through the U.S. National Science Foundation (NSF) under Cooperative Agreement OAC-1836650. J. D. is supported by the U.S. Department of Energy (DOE), Office of Science, Office of High Energy Physics Early Career Research program under Award No. DE-SC0021187. G. D. is supported by DOE Award No. DE-SC0007968. We gratefully acknowledge the input and discussion from the Exa.TrkX collaboration.

References

- [1] G. Piacquadio, K. Prokofiev, A. Wildauer, J. Phys. Conf. Ser. **119**, 032033 (2008)
- [2] S. Chatrchyan et al. (CMS), JINST **9**, P10009 (2014), 1405.6569
- [3] M. Aaboud et al. (ATLAS), Eur. Phys. J. C **77**, 466 (2017), 1703.10485
- [4] A. Sirunyan et al. (CMS), JINST **12**, P10003 (2017), 1706.04965
- [5] A.J. Larkoski, I. Moutl, B. Nachman, Phys. Rept. **841**, 1 (2020), 1709.04464
- [6] A.M. Sirunyan et al. (CMS), JINST **13**, P05011 (2018), 1712.07158
- [7] M. Aaboud et al. (ATLAS), JHEP **08**, 089 (2018), 1805.01845
- [8] S. Chatrchyan et al. (CMS), JINST **9**, P10009 (2014), 1405.6569
- [9] M. Aaboud, G. Aad, B. Abbott, J. Abdallah, O. Abdinov, B. Abeloos, S.H. Abidi, O.S. AbouZeid, N.L. Abraham, et al., The European Physical Journal C **77** (2017)
- [10] P. Billoir, Comput. Phys. Comm. **57**, 390 (1989)
- [11] P. Billoir, S. Qian, Nucl. Instrum. Meth. A **294**, 219 (1990)
- [12] R. Mankel, Nucl. Instrum. Meth. A **395**, 169 (1997)
- [13] R. Frühwirth, Nucl. Instrum. Meth. A **262**, 444 (1987)
- [14] CMS Note CMS-NOTE-2018-006. CERN-CMS-NOTE-2018-006 (2018), <https://cds.cern.ch/record/2650976>
- [15] **4/2017** (2017)
- [16] M.M. Bronstein, J. Bruna, Y. LeCun, A. Szlam, P. Vandergheynst, IEEE Signal Process. Mag. **34**, 18 (2017), 1611.08097
- [17] Z. Zhang, P. Cui, W. Zhu (2020), 1812.04202
- [18] J. Zhou, G. Cui, Z. Zhang, C. Yang, Z. Liu, L. Wang, C. Li, M. Sun (2019), 1812.08434
- [19] Z. Wu, S. Pan, F. Chen, G. Long, C. Zhang, P.S. Yu, IEEE Trans. Neural Netw. Learn. Syst. p. 1 (2020), 1901.00596
- [20] F. Scarselli, M. Gori, A.C. Tsoi, M. Hagenbuchner, G. Monfardini, IEEE Trans. Neural Netw. **20**, 61 (2009)
- [21] C.R. Qi, H. Su, K. Mo, L.J. Guibas, *PointNet: Deep Learning on Point Sets for 3D Classification and Segmentation*, in *2017 IEEE Conference on Computer Vision and Pattern Recognition (CVPR)* (2017), 1612.00593
- [22] J. Gilmer, S.S. Schoenholz, P.F. Riley, O. Vinyals, G.E. Dahl, *Neural message passing for quantum chemistry*, in *Proceedings of the 34th International Conference on Machine Learning* (2017), Vol. 70 of *Proceedings of Machine Learning Research*, p. 1263, 1704.01212, <http://proceedings.mlr.press/v70/gilmer17a.html>
- [23] P.W. Battaglia, R. Pascanu, M. Lai, D.J. Rezende, K. Kavukcuoglu, *Interaction Networks for Learning about Objects, Relations and Physics*, in *Advances in Neural Information Processing Systems 29*, edited by D. Lee, M. Sugiyama, U. Luxburg, I. Guyon, R. Garnett (Curran Associates, Inc., 2016), Vol. 29, p. 4502, 1612.00222, <https://papers.nips.cc/paper/2016/hash/3147da8ab4a0437c15ef51a5cc7f2dc4-Abstract.html>
- [24] P.W. Battaglia et al. (2018), 1806.01261
- [25] Y. Wang, Y. Sun, Z. Liu, S.E. Sarma, M.M. Bronstein, J.M. Solomon, ACM Trans. Graph. **38** (2019), 1801.07829
- [26] S. Farrell et al., *Novel deep learning methods for track reconstruction*, in *4th International Workshop Connecting The Dots 2018* (2018), 1810.06111
- [27] X. Ju et al., *Graph Neural Networks for Particle Reconstruction in High Energy Physics Detectors*, in *Machine Learning and the Physical Sciences Workshop at the 33rd Annual*

- Conference on Neural Information Processing Systems* (2019), 2003.11603, https://ml4physicalsciences.github.io/files/NeurIPS_ML4PS_2019_83.pdf
- [28] A. Heintz, V. Razavimaleki, J. Duarte, G. DeZoort, I. Ojalvo, S. Thais, M. Atkinson, M. Neubauer, L. Gray, S. Jindariani et al., *Accelerated charged particle tracking with graph neural networks on FPGAs*, in *3rd Machine Learning and the Physical Sciences Workshop at the 34th Annual Conference on Neural Information Processing Systems* (2020), 2012.01563, https://ml4physicalsciences.github.io/2020/files/NeurIPS_ML4PS_2020_137.pdf
- [29] M. Besta, D. Stanojevic, J. de Fine Licht, T. Ben-Nun, T. Hoefler (2019), 1903.06697
- [30] A. Strandlie, R. Frühwirth, *Rev. Mod. Phys.* **82**, 1419 (2010)
- [31] S. Amrouche et al., *The Tracking Machine Learning Challenge: Accuracy Phase*, in *The NeurIPS '18 Competition* (2020), p. 231, ISBN 978-3-030-29135-8, 1904.06778
- [32] M. Ester, H.P. Kriegel, J. Sander, X. Xu, *A Density-Based Algorithm for Discovering Clusters in Large Spatial Databases with Noise*, in *Proceedings of the Second International Conference on Knowledge Discovery and Data Mining* (AAAI Press, 1996), p. 226, <https://www.aaai.org/Papers/KDD/1996/KDD96-037.pdf>
- [33] A. Paszke, S. Gross, F. Massa, A. Lerer, J. Bradbury, G. Chanan, T. Killeen, Z. Lin, N. Gimelshein, L. Antiga et al., *PyTorch: An Imperative Style, High-Performance Deep Learning Library*, in *Advances in Neural Information Processing Systems*, edited by H. Wallach, H. Larochelle, A. Beygelzimer, F. d'Alché-Buc, E. Fox, R. Garnett (Curran Associates, Inc., 2019), Vol. 32, 1912.01703, <https://proceedings.neurips.cc/paper/2019/file/bdbca288fee7f92f2bfa9f7012727740-Paper.pdf>
- [34] V. Nair, G.E. Hinton, *Rectified Linear Units Improve Restricted Boltzmann Machines*, in *27th International Conference on International Conference on Machine Learning* (Omnipress, Madison, WI, USA, 2010), ICML'10, p. 807, ISBN 9781605589077
- [35] X. Glorot, A. Bordes, Y. Bengio, *Deep Sparse Rectifier Neural Networks*, in *14th International Conference on Artificial Intelligence and Statistics*, edited by G. Gordon, D. Dunson, M. Dudík (JMLR, Fort Lauderdale, FL, USA, 2011), Vol. 15, p. 315, <http://proceedings.mlr.press/v15/glorot11a.html>
- [36] D.P. Kingma, J. Ba, *Adam: A Method for Stochastic Optimization*, in *3rd International Conference on Learning Representations*, edited by Y. Bengio, Y. LeCun (2015), 1412.6980
- [37] M.M.A. Patwary, J. Blair, F. Manne, *Experiments on Union-Find Algorithms for the Disjoint-Set Data Structure*, in *Experimental Algorithms*, edited by P. Festa (Springer Berlin Heidelberg, Berlin, Heidelberg, 2010), pp. 411–423, ISBN 978-3-642-13193-6
- [38] J. Krupa, K. Lin, M.A. Flechas, J. Dinsmore, J. Duarte, P. Harris, S. Hauck, B. Holzman, S.C. Hsu, T. Klijnsma et al. (2020), submitted to *Mach. Learn.: Sci. Technol.*, 2007.10359
- [39] D.S. Rankin, J. Krupa, P. Harris, M.A. Flechas, B. Holzman, T. Klijnsma, K. Pedro, N. Tran, S. Hauck, S.C. Hsu et al., *FPGAs-as-a-Service Toolkit (FaaS_T)*, in *2020 IEEE/ACM International Workshop on Heterogeneous High-performance Reconfigurable Computing (H2RC)* (2020), 2010.08556
- [40] M. Wang, T. Yang, M. Acosta Flechas, P. Harris, B. Hawks, B. Holzman, K. Knoepfel, J. Krupa, K. Pedro, N. Tran, *Front. Big Data* **3**, 48 (2021), 2009.04509
- [41] Y. Umuroglu, N.J. Fraser, G. Gambardella, M. Blott, P. Leong, M. Jahre, K. Vissers, *FINN: A Framework for Fast, Scalable Binarized Neural Network Inference*, in *Proceedings of the 2017 ACM/SIGDA International Symposium on Field-Programmable Gate Arrays* (ACM, New York, NY, USA, 2017), p. 65, ISBN 9781450343541,

- [42] M. Blott, T. Preußner, N. Fraser, G. Gambardella, K. O'Brien, Y. Umuroglu, *ACM Trans. Reconfigurable Technol. Syst.* **11** (2018), 1809.04570
- [43] A. Shawahna, S.M. Sait, A. El-Maleh, *IEEE Access* **7**, 7823 (2019), 1901.00121
- [44] T. Wang, C. Wang, X. Zhou, H. Chen, *An Overview of FPGA Based Deep Learning Accelerators: Challenges and Opportunities*, in *2019 IEEE 21st International Conference on High Performance Computing and Communications; IEEE 17th International Conference on Smart City; IEEE 5th International Conference on Data Science and Systems (HPCC/SmartCity/DSS)* (2019), p. 1674, 1901.04988
- [45] J. Duarte et al., *JINST* **13**, P07027 (2018), 1804.06913
- [46] S. Summers et al., *JINST* **15**, P05026 (2020), 2002.02534
- [47] J. Ngadiuba et al., *Mach. Learn.: Sci. Technol.* **2**, 015001 (2020), 2003.06308
- [48] C.N. Coelho, A. Kuusela, S. Li, H. Zhuang, T. Aarrestad, V. Loncar, J. Ngadiuba, M. Pierini, A.A. Pol, S. Summers (2020), submitted to *Nat. Mach. Intell.*, 2006.10159
- [49] T. Aarrestad et al. (2021), submitted to *Mach. Learn.: Sci. Technol.*, 2101.05108
- [50] Y. Iiyama et al., *Front. Big Data* **3**, 44 (2021), 2008.03601
- [51] B. Moons, K. Goetschalckx, N.V. Berckelaer, M. Verhelst, *Minimum Energy Quantized Neural Networks*, in *2017 51st Asilomar Conference on Signals, Systems, and Computers* (2017), p. 1921, 1711.00215
- [52] M. Courbariaux, Y. Bengio, J.P. David, *BinaryConnect: Training Deep Neural Networks with binary weights during propagations*, in *Advances in Neural Information Processing Systems*, edited by C. Cortes, N.D. Lawrence, D.D. Lee, M. Sugiyama, R. Garnett (Curran Associates, Inc., 2015), Vol. 28, p. 3123, 1511.00363, <https://proceedings.neurips.cc/paper/2015/file/3e15cc11f979ed25912dff5b0669f2cd-Paper.pdf>
- [53] D. Zhang, J. Yang, D. Ye, G. Hua, *LQ-nets: Learned quantization for highly accurate and compact deep neural networks*, in *Proceedings of the European Conference on Computer Vision (ECCV)* (2018), p. 365, 1807.10029
- [54] F. Li, B. Liu (2016), 1605.04711
- [55] S. Zhou, Y. Wu, Z. Ni, X. Zhou, H. Wen, Y. Zou (2016), 1606.06160
- [56] I. Hubara, M. Courbariaux, D. Soudry, R. El-Yaniv, Y. Bengio, *J. Mach. Learn. Res.* **18**, 1 (2018), 1609.07061
- [57] M. Rastegari, V. Ordonez, J. Redmon, A. Farhadi, *XNOR-Net: ImageNet Classification Using Binary Convolutional Neural Networks*, in *14th European Conference on Computer Vision (ECCV)* (Springer International Publishing, Cham, Switzerland, 2016), p. 525, 1603.05279
- [58] P. Micikevicius, S. Narang, J. Alben, G. Diamos, E. Elsen, D. Garcia, B. Ginsburg, M. Houston, O. Kuchaiev, G. Venkatesh et al., *Mixed precision training*, in *6th International Conference on Learning Representations* (2018), 1710.03740, <https://openreview.net/forum?id=r1gs9JgRZ>
- [59] B. Zhuang, C. Shen, M. Tan, L. Liu, I. Reid, *Towards Effective Low-Bitwidth Convolutional Neural Networks*, in *2018 IEEE/CVF Conference on Computer Vision and Pattern Recognition* (2018), p. 7920, 1711.00205
- [60] N. Wang, J. Choi, D. Brand, C.Y. Chen, K. Gopalakrishnan, *Training deep neural networks with 8-bit floating point numbers*, in *Advances in Neural Information Processing Systems*, edited by S. Bengio, H. Wallach, H. Larochelle, K. Grauman, N. Cesa-Bianchi, R. Garnett (Curran Associates, Inc., 2018), Vol. 31, p. 7675, 1812.08011, <https://proceedings.neurips.cc/paper/2018/file/>

335d3d1cd7ef05ec77714a215134914c-Paper.pdf

- [61] C. Coelho, *QKeras* (2019), <https://github.com/google/qkeras>
- [62] A. Pappalardo, *Xilinx/brevitas* (2020), <https://doi.org/10.5281/zenodo.3333552>
- [63] Y. LeCun, J.S. Denker, S.A. Solla, *Optimal Brain Damage*, in *Advances in Neural Information Processing Systems 2*, edited by D.S. Touretzky (Morgan-Kaufmann, 1990), p. 598, <http://papers.nips.cc/paper/250-optimal-brain-damage>
- [64] S. Han, H. Mao, W.J. Dally, *Deep Compression: Compressing Deep Neural Networks with Pruning, Trained Quantization and Huffman Coding*, in *4th International Conference on Learning Representations* (2016), 1510.00149
- [65] J. Frankle, M. Carbin, *The Lottery Ticket Hypothesis: Training Pruned Neural Networks*, in *7th International Conference on Learning Representations* (2019), 1803.03635, <https://openreview.net/forum?id=rJl-b3RcF7>
- [66] H. Zhou, J. Lan, R. Liu, J. Yosinski, *Deconstructing Lottery Tickets: Zeros, Signs, and the Supermask*, in *Advances in Neural Information Processing Systems*, edited by H. Wallach, H. Larochelle, A. Beygelzimer, F. d'Alché Buc, E. Fox, R. Garnett (Curran Associates, Inc., 2019), Vol. 32, p. 3597, 1905.01067, <https://proceedings.neurips.cc/paper/2019/file/1113d7a76ffceca1bb350bfe145467c6-Paper>
- [67] D. Blalock, J.J.G. Ortiz, J. Frankle, J. Gutttag, *What is the State of Neural Network Pruning?*, in *4th Conference on Machine Learning and Systems* (2020), 2003.03033
- [68] B. Hawks, J. Duarte, N.J. Fraser, A. Pappalardo, N. Tran, Y. Umuroglu (2021), 2102.11289
- [69] V. Loncar, S. Summers, N. Tran, B. Kreis, J. Duarte, jngadiub, D. Hoang, E. Kreinar, A.A. Pol, D. Golubovic et al., *fastmachinelearning/hls4ml* (2021)
- [70] S.R. Qasim, J. Kieseler, Y. Iiyama, M. Pierini, *Eur. Phys. J. C* **79**, 608 (2019), 1902.07987
- [71] A. Vaswani, N. Shazeer, N. Parmar, J. Uszkoreit, L. Jones, A.N. Gomez, Ł. Kaiser, I. Polosukhin, *Attention Is All You Need*, in *Advances in Neural Information Processing Systems*, edited by I. Guyon, U.V. Luxburg, S. Bengio, H. Wallach, R. Fergus, S. Vishwanathan, R. Garnett (Curran Associates, Inc., 2017), Vol. 30, p. 5998, 1706.03762, <https://proceedings.neurips.cc/paper/2017/file/3f5ee243547dee91fbd053c1c4a845aa-Paper.pdf>
- [72] N. Kitaev, Ł. Kaiser, A. Levskaya, *Reformer: The Efficient Transformer*, in *8th International Conference on Learning Representations* (2020), 2001.04451, <https://openreview.net/forum?id=rkgNKkHtvB>
- [73] K. Choromanski, V. Likhoshesterov, D. Dohan, X. Song, A. Gane, T. Sarlos, P. Hawkins, J. Davis, A. Mohiuddin, L. Kaiser et al., *Rethinking Attention with Performers*, in *International Conference on Learning Representations* (2021), 2009.14794, <https://openreview.net/forum?id=Ua6zuk0WRH>